Dynamic Thermal-Regulating Textiles with Metallic Fibers Based on a Switchable Transmittance

Muluneh G. Abebe[◉],[1,][*] Gilles Rosolen,[1] Eric Khousakoun,[2] Jeremy Odent[◉],[3] Jean-Marie Raquez,[3] Sylvain Desprez,[2] and Bjorn Maes[1]

[1]*Micro- and Nanophotonic Materials Group, Research Institute for Materials Science and Engineering, University of Mons, 20 Place du Parc, Mons B-7000, Belgium*
[2]*Materia Nova, Avenue N. Copernic 3, Mons B-7000, Belgium*
[3]*Laboratory of Polymeric and Composite Materials, University of Mons, 20 Place du Parc, Mons B-7000, Belgium*

Personal radiative thermal management using photonic smart textiles has become a center of attention due to its potential to facilitate thermal comfort, and to decrease the energy cost for heating and cooling. Here, we provide an approach for a dynamic transmittance switch textile (DTST): a dynamic, passive, radiative thermal regulating fabric that controls the infrared (IR) transmission by adapting to the ambient temperature and humidity. The DTST is constituted from metal-coated monofilaments and stimuli-responsive polymer actuator beads, in this way benefiting from multiple IR photonic effects to strongly control the wide-band transmission of thermal radiation and to provide for a sharp, dynamic response. This design shows a wide dynamic ambient setpoint temperature window of approximately 16 °C, meaning that the wearer is comfortable between 9.5 and 25.7 °C, wider than any theoretically reported or fabricated switchable fabric. This performance indicates a polyvalent user comfort and an important energy saving potential for residential and office buildings.

DOI: 10.1103/PhysRevApplied.14.044030

I. INTRODUCTION AND MOTIVATION

Recently, natural disasters due to extreme weather conditions have become frequent events in some parts of the world. There is mounting evidence that these events relate to the Earth's climate change and global warming [1,2]. As far as humankind is concerned, global warming imposes a severe existential threat and has to be addressed [3–5]. Even though there are various human-induced factors, the imbalance between the increasing energy consumption and clean energy production stands out. Because of this, the rapid switch to renewable energy sources is difficult, and solutions to significantly decrease the energy consumption are crucial. From the total global energy consumption, a substantial amount (approximately 50%) is used in commercial and residential buildings for heating and cooling purposes [6,7]. Recently, passive and active personal thermal management using smart textiles, which provide a localized thermal regulation, has become an excellent candidate to save energy.

At a normal skin temperature of 34 °C, our skin emits infrared radiation (IR) with a peak wavelength around 9.6 μm. This IR heat dissipation channel contributes to more than 50% of the total body heat loss in indoor

environments [8]. Therefore, with proper IR management, one can tailor and design both active and passive radiative thermal regulating textiles.

State-of-the-art *active* radiative thermal regulating textiles have a dynamic switching capability, thus allowing both a heating and cooling functionality simultaneously [9]. However, this technology requires an external input, such as an applied voltage or mechanical pressure, resulting in energy consumption. On the other hand, *passive* radiative thermal regulating textiles do not require any external input to operate, making them a better, sustainable choice. Thus far, most of the reported passive radiative thermal regulating textiles are nonresponsive to environmental changes, lacking a dynamic nature to regulate heating and cooling functionalities [10–29].

Although extensive research has been devoted to the design of a dynamic and passive radiative thermal management textile, to date, it remains a considerable challenge. Among the state-of-the-art fabrics, Zhang *et al.* [30] designed and fabricated a textile that uses bimorph fibers coated with carbon nanotubes to dynamically control the IR emissivity. The major drawback is that the dynamic nature of the fabric can only be triggered by humidity, such that the user has to sweat for actuation, causing discomfort. Another state-of-the-art fabric is reported by Hsu *et al.* [31], a dual-mode textile designed and fabricated to

―――――――
[*]mulunehgeremew.abebe@umons.ac.be

provide both heating and cooling functionalities, based on different emissivities of the outer fabric surface. However, one has to flip the textile to switch between the distinct modes.

In this work, we provide a promising framework for a dynamic transmittance switch textile (DTST) technology: a dynamic, passive, radiative thermal regulating fabric that controls the IR transmission by adapting to the ambient temperature and humidity. The dynamic transmittance modulates the thermal heat transfer between the human body and the ambient environment, which is vital for the wearer's comfort. We perform a careful numerical study of the photonic properties of the design, in order to determine optimized geometric parameters for both a heating and cooling functionality. The dynamic switchable transmittance is achieved by utilizing the diverse photonic band gaps exhibited due to the design geometry and material properties of a metallic coating. The functionality mainly capitalizes on the metallic photonic effect (or plasmonic gap), and its spectral properties shift as a function of the design parameters. Furthermore, with thermal calculations, we determine that a woven-configuration DTST shows an approximately $16\,^{\circ}\mathrm{C}$ ambient setpoint temperature window, which is very large compared to previously reported technologies.

In Sec. II A we provide a detailed explanation of the working principle of the proposed technology. In Sec. II B we introduce the electromagnetic calculations, scaling method, and figures of merit. In Secs. III A and III B we assess the results from electromagnetic calculations for transverse-electric (TE) and transverse-magnetic (TM) polarizations, and further evaluate these findings for flexible textiles in Sec. III C. In Sec. III D we evaluate the potential of the technology based on thermal calculations, and in Sec. IV we conclude the paper.

II. DESIGN AND METHOD

A. Design working principle

The DTST fabric incorporates monofilaments coated with a conductive material, which are arranged in a photonic array geometry in a suitable combination with a shape-memory polymer. The concept builds on the following factors: material properties (i.e., scattering properties of the metallic coating, thermal and mechanical properties of the stimuli-responsive polymer actuator), design geometry (i.e., shape and arrangement of the monofilaments), and environmental factors (i.e., relative temperature and humidity).

Here, a metal is used as a coating material due to its high reflectivity in the wavelength range of human body emission. In contrast, with dielectric monofilaments (without metal) below an optimum diameter, the IR transmission would rapidly increase, as large wavelengths only weakly interact. However, due to conductivity, metal-coated monofilaments act like little antennae, which scatter and strongly interact with IR radiation, even if the monofilament diameter is much smaller than the wavelength. In this way, a strong IR transmission control is possible, with efficient thermal body regulation, as shown later. Metals such as silver, gold, and aluminum can all be used as a coating on a dielectric-core monofilament, which can be composed of natural or synthetic textile materials such as cotton and polyester.

In Fig. 1 we show the detailed mechanism of the DTST, in comparison with a traditional textile fabric. Traditional textiles [Fig. 1(a)] can only be used comfortably in a limited window with respect to temperature and humidity. In cold weather, the temperature of the human body is higher than the ambient temperature, and this leads to radiative heat loss from the body. Thus, one can utilize

(a) Static (traditional textile fabric)   **(b)**   Dynamic (DTST fabric)

One mode
IR transmission
Human body IR radiation

(i) Heating mode: cold, $T < T_c$
Low IR transmission
Metal-coated monofilament
Shrank polymer blobs
Human body IR radiation

(ii) Cooling mode: hot, $T > T_c$
High IR transmission
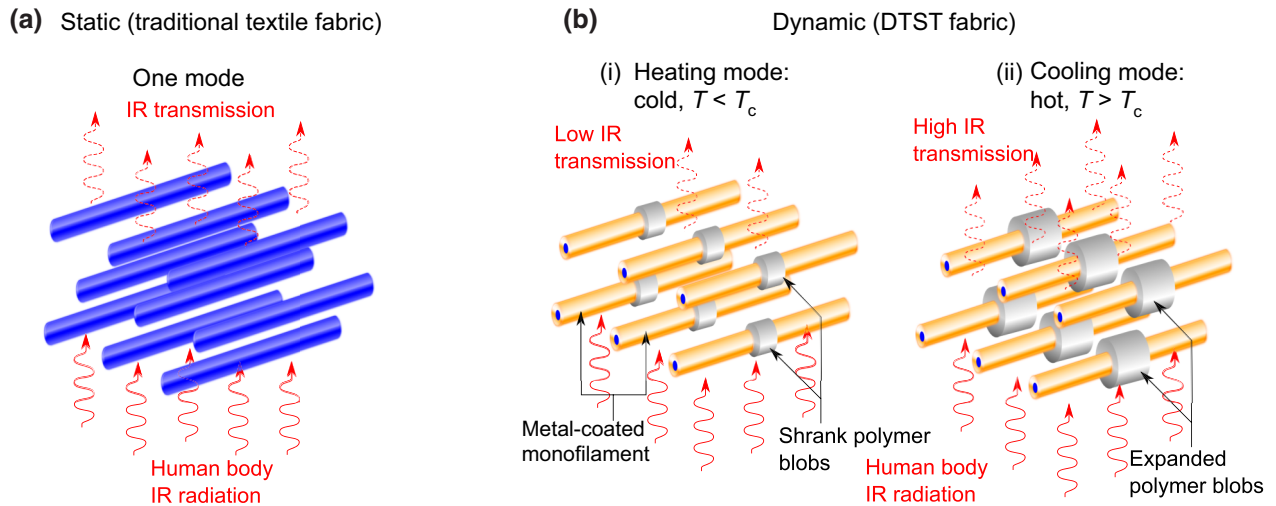Human body IR radiation
Expanded polymer blobs

FIG. 1. Comparison of traditional textile with the DTST principle. (a) Traditional textile fabric with a single-mode, static operation, (b) DTST with dynamic two-mode flexibility: (i) heating and (ii) cooling.

a warm winter cloth that blocks the heat loss from the body and benefit from the warming nature of the fabric (e.g., with low IR transmittance). On the other hand, in hot weather conditions, one needs a summer cloth that allows the human body to relieve heat stress (e.g., with high IR transmittance). However, it is impossible to use a single static fabric comfortably in both weather conditions, which restricts their performance: there is no adaptation to a changing environment, with only a fixed function (e.g., IR transmittance) by design.

With the DTST [Fig. 1(b)] there are two modes: a heating mode for warming functionality (low IR transmittance) and a cooling mode for cooling functionality (high IR transmittance). These two modes coexist simultaneously in the fabric, with a passive switching mechanism to change from one mode to the other. Here, stimuli-responsive polymer actuator beads in between the fibers are proposed as a driving force for passive switching [32]. More specifically, a well-trained reversible two-way thermo-humidity responsive shape-memory polymer creates the operation mechanism. These polymers are dual-shape materials that belong to the group of actively moving polymers, and change from a shape X to another shape Y. Shape X is a temporary shape that is obtained by mechanical deformation and subsequent fixation of that deformation [33–36]. Thus, such materials have the ability to return from the temporary shape X to their original shape Y in a short time after an external stimulus, and in our case, deviations in temperature and humidity can be exploited. Recent studies have reported that polymers such as bio-based polylactide urethane [37], polyurethane [38,39], and other polymers [40,41] show programmed shape-memory properties around the human body temperature. Therefore, the proposed polymer beads can be made from these types of materials. Note that care must be taken while choosing the right polymer actuator. Essentially, even though sensitivity to temperature and humidity are the basic criteria, a significant IR transparency must be ensured for the radiative functionality.

For example, at a predetermined comfort zone temperature and humidity below a critical temperature T_c and critical humidity H_c, the polymer beads determine a particular fiber geometry. When the temperature rises above T_c (or humidity above H_c), the polymer beads expand, thus increasing the separation distance d (Fig. 2) between two neighboring monofilaments. This results in a new geometric configuration with an expected increased IR transmittance, and a subsequent increase in radiative heat transfer to the environment. On the other hand, when the ambient temperature and humidity drop below T_c and H_c, the polymer shrinks, thus decreasing d. As a result, the geometric configuration will change, and the IR transmittance is expected to decrease, thus reducing the radiative heat loss. Thus, the DTST provides a dynamic, passive cooling and heating functionality by facilitating or
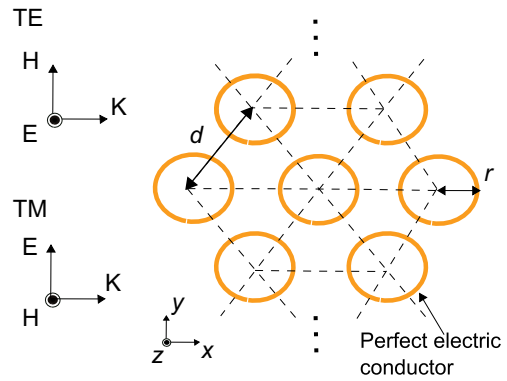

FIG. 2. The simulated model for the IR response: d denotes the separation distance between two neighboring monofilaments, r denotes the radius. The polarization convention and incidence direction are indicated. The pattern is repeated in the vertical y direction. H, magnetic field; E, Electric field; K, Wave vector.

suppressing the radiative heat transfer generated by the human body.

B. Electromagnetic modeling

We implement two steps for calculating the essential IR optical response of the proposed textile design. First, we implement an electromagnetic simulation for a specific geometry with a fixed wire separation distance d, and a varying filling ratio $f = 2r/d$, where r is the radius of the monofilament (Fig. 2). Second, by benefiting from the scale invariance property of Maxwell's equations, we rapidly compute spectra for an extended set of d values. The latter procedure significantly speeds up the process, so we can calculate an integrated figure of merit over a wide range of geometric parameters.

1. Simulation setup

To study the IR transmission of the design, we employ the finite-element method to calculate rigorous solutions of Maxwell's equations, using commercial software (COMSOL Multiphysics® v5.3). Since the metal-coated monofilaments are considered infinitely long, identical, parallel cylinders, the geometry is two dimensional, consisting of an array of circular, metal-coated monofilaments, hexagonally arranged and surrounded by air (Fig. 2). We use air as the background medium, as the shape-memory polymer beads take only a very small volume in the structure. Moreover, the refractive index of such polymers, typically below 1.5, would only slightly increase the effective index.

In the relevant IR wavelength range, many metals can be approximated as perfect electric conductors, with an infinite conductivity. Thus, we can implement the perfect electric conductor (PEC) boundary condition around the monofilaments. This leads to a complete reflection of incident radiation from these surfaces, without any material losses. Floquet periodic boundary conditions are used on

the top and bottom boundaries, to represent an infinite repetition in the vertical direction of Fig. 2. The various diffraction orders that originate for smaller wavelength excitations are computed with port conditions (on the left and right sides of Fig. 2).

A plane-wave source with perpendicular incidence impinges upon the structure. The IR transmittance depends strongly on the polarization of the incident radiation. Therefore, it is of crucial importance to take into account both a TE (one electric field component out of plane) and TM (one magnetic field component out of plane) case. After calculating the transmission spectra, we determine the figure of merit τ given by

$$\tau = \frac{\int_{\lambda_1}^{\lambda_2} T(\lambda)\phi_{bb}(\lambda)\,d\lambda}{\int_{\lambda_1}^{\lambda_2} \phi_{bb}(\lambda)\,d\lambda}, \tag{1}$$

where T is the transmission spectrum of the fabric, ϕ_{bb} is Planck's black body distribution for a skin temperature at $34\,^\circ$C, and (λ_1, λ_2) is the wavelength interval that covers nearly all of the human body emission spectrum (we use 4–45 μm). Hence, τ will be used throughout this work as a standard measure of how much emitted thermal radiation by the human body is transmitted through the fabric to the ambient environment.

2. Scaling

A large parameter range needs to be studied: distance $d = 0.4$–18 μm, filling factor $f = 0.01$–0.5, and the whole wavelength range of human body emission (4–45 μm). Most of the recent literature uses 5–25 μm for the wavelength range; however, more than 15% of thermal body radiation is above 25 μm, so we employ a wider range. We vary f from 0.01 to 0.5 in steps of 0.025 for a fixed value of d, leading to simulations of 20 different geometries for a single d. Each simulation requires extensive computational time and memory, but we can fortunately limit the number of simulations by exploiting a scaling method.

In classical electromagnetism the field equations are scale invariant in the absence of any source (i.e., charge and current). Specifically, Maxwell's equations are invariant under the transformations $x - \lambda x$ and $t - \lambda t$, so solutions of a micrometer-scale structure at IR wavelengths are the same as those for the nanometer-scale structure at optical wavelengths (without material dispersion). By following this principle we develop a scaling technique to procure all the solutions for $d = 0.4$–18 μm using the result from a single simulation at $d = 10$ μm.

The use of PEC conditions allows us to implement the scaling method, as, in principle, real metals with wavelength-dependent or dispersive electromagnetic properties break the invariance. However, the scaling approach remains highly accurate for our IR situation, where real metals are highly conductive. Indeed, we compared simulations with metals (such as silver) and PEC conditions, and the results are quasi-identical (see Fig. 2 within the Supplemental Material [42]).

III. RESULTS AND DISCUSSION

We discuss in detail the electromagnetic calculation results for both TE (Sec. III A) and TM (Sec. III B) polarizations, leading to qualitative differences between the cases. Furthermore, we discuss these electromagnetic findings for dynamic textile applications (Sec. III C). Finally, we evaluate the overall efficiency with respect to the user's thermal comfort, which is strongly enhanced (Sec. III D).

A. TE polarization

As we will see, the TE transmission spectra are very distinctive, and provide good opportunities for thermal tuning. Simulations of TE transmittance are shown in Fig. 3 for selected parameters: each panel fixes f and shows spectra with varying d. The spectra have specific wavelength regions or bands due to a number of photonic effects. Note a similarity between the curves, with varying band
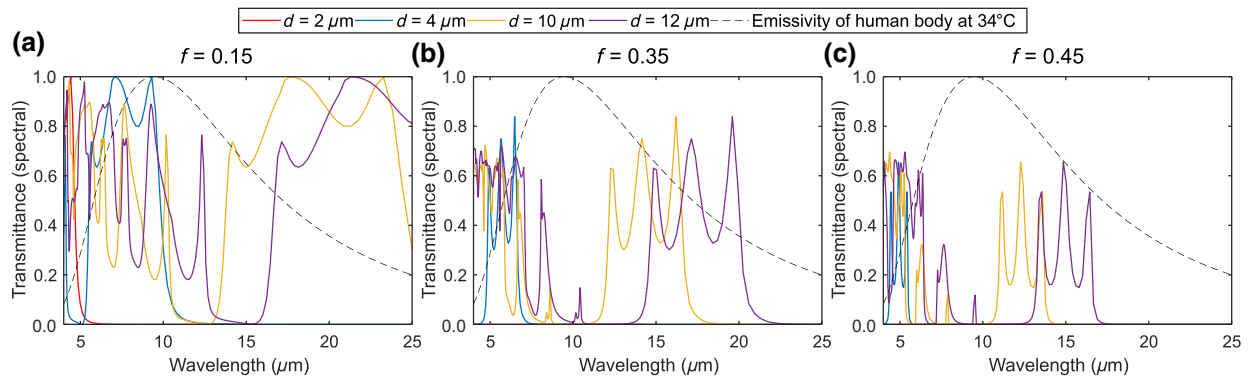

FIG. 3. Simulations of TE transmittance as a function of wavelength for $d = 2, 4, 10,$ and 12 μm and (a) $f = 0.15$, (b) $f = 0.35$, (c) $f = 0.45$ (solid lines). The dashed line depicts the human body emissivity at a skin temperature of $34\,^\circ$C.

positions along the wavelength axis (shifting to right or left) and band magnitudes (higher or lower transmittance).

For a clear example, we examine the curve for $d = 10$ μm in Fig. 3(b) ($f = 0.35$, orange line). For larger wavelengths, above a cutoff wavelength of about 17 μm, the spectrum exhibits a wide (semi-infinite) stopband with low transmission, called the plasmonic gap, leading to a complete blockage of thermal radiation transmission [43–47]. Interestingly, this gap does not originate from the geometry of the design, but rather from the physical property of the perfectly conducting scatterers [48].

Next to the plasmonic gap, there is a first transmission band, extending from 12 to 17 μm, with a center wavelength following the Bragg condition, similar to dielectric photonic crystal band gaps [49]. This transmission band presents three resonance peaks, similar to Fabry-Pérot cavity modes of finite photonic crystals or multilayers with only a few layers [48,50].

In addition to the plasmonic gap, we observe a structural band gap for wavelengths just below the first transmission band [51,52], which originates from the geometric design, and extends from 9 to 12 μm, again blocking the transmission of thermal radiation. Finally, below the structural band gap, there is a continuous second transmission band below 9 μm, with a complicated set of resonances.

Now we can assess the impact of d and f on these particular ranges. When d increases (decreases), the spectra shift to longer (shorter) wavelengths. For example, for $f = 0.35$ [Fig. 3(b)], when increasing d from 10 to 12 μm, the spectrum shifts to the right: plasmonic gap (from greater than 17 μm to greater than 22 μm), first transmission band (from 12–17 μm to 14–21 μm), structural band gap (from 9–12 μm to 11–14 μm), and second transmission band (from less than 9μm to less than 11 μm).

For the effect of the fill factor f, we can compare, e.g., the three spectra for $d = 10$ μm [orange graphs in Figs. 3(a)–3(c) for $f = 0.15$, 0.35, and 0.45]. Overall, the magnitude of the transmission bands decreases when f increases, as we indeed expect more scattering.

Furthermore, if we examine the first transmission band, the large wavelength edge shifts much more than the small wavelength edge. Consequently, for increasing f, the first transmission band becomes noticeably narrower. The structural band gap, however, remains fairly constant in width.

The variations of d and f thus have significant consequences, especially concerning band shifting. This effect is imperative for the dynamic fabric, as the human body emissivity is fixed (dashed black line in Fig. 3), while the textile transmission can switch by tuning d and f. Now, we need to find optimal parameter values that allow the fabric to operate efficiently in two different modes (cooling and heating modes), for which we use the integrated transmittance τ [see Eq. (1)] as a figure of merit, with the integration performed over the emissivity of the human body ($\lambda_1 = 4$ μm, $\lambda_2 = 45$ μm) at a skin temperature of 34 °C.

In Fig. 4(a) we map τ as a function of d and f, where we can distinguish five regions: (i) bottom-left corner where both f and d are very small ($f < 0.1$, $d < 2$ μm), (ii) bottom-right corner where f is large and d is relatively small ($f > 0.4$ and $d < 2$ μm), (iii) top-left corner where f is small and d is large ($f < 0.1$ and $d > 10$ μm), (iv) top-right corner where both f and d are very large, (v) the middle where d is from 2 to 10 μm and the whole range of $f = 0.02$ to 0.45. We now discuss these regions, with an eye to dynamic textile application.

In region (i), τ is close to zero, and this implies that, when both f and d are small, the proposed design will reflect most of the thermal radiation back to the human body. As a result, the DTST is operating in a heating mode. The very low τ in this region is because the plasmonic gap shifts to short wavelengths, as far as below 5 μm [see $d = 2$ μm (red curve) in Fig. 3(a)], covering most of the human body emissivity curve. So the first transmission band has almost no overlap with the human emissivity, resulting in a very low τ.

In region (ii), τ becomes even smaller. With increasing f, the transmission band becomes weaker, and shifts even
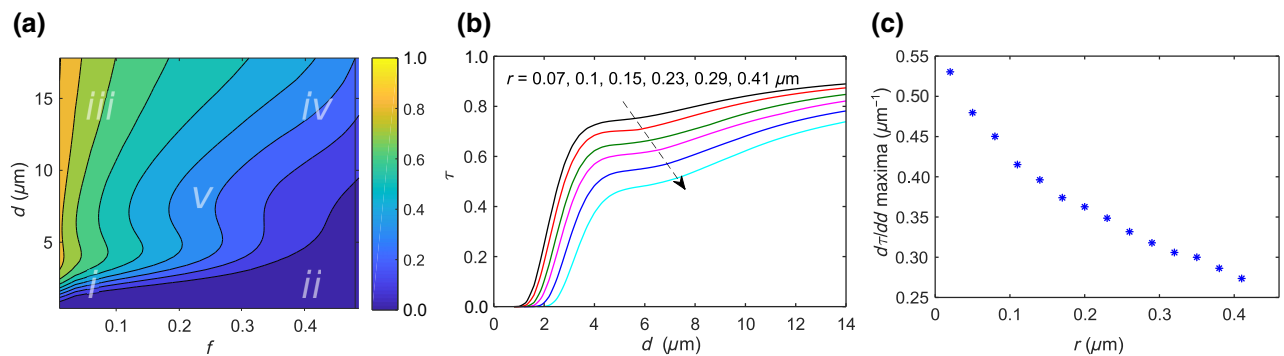

FIG. 4. Spectrally integrated transmittance τ for TE polarization. (a) Map showing τ as a function of f and d. (b) Plot of τ as a function of d for constant radii r. (c) The maximum of $d\tau/dd$ as a function of r.

further to smaller wavelengths, leading to even less overlap. Therefore, the fabric can operate in the heating mode in this region as well, profiting from the plasmonic gap.

In region (iii), τ is above 0.7 due to a large d and small f, which fosters the dominance of the second transmission band. In this case, both the plasmonic gap and the structural band gap are shifted towards larger wavelengths, beyond the main human body emissivity range. Therefore, thermal radiation transmission from the human body to the environment increases; thus, this region can facilitate a cooling mode.

Region (iv) presents a moderate τ, in the range of 0.4 to 0.5. In this case, the important second transmission band due to increased d is counterbalanced by the decrease of the magnitude of this specific band due to an increase in f. In addition, the structural band gap broadens due to f. Moreover, the plasmonic gap shifts to shorter wavelengths, decreasing τ [see $d = 12$ μm (purple curve) in Figs. 3(a)–3(c)].

In region (v) there is a bump around $d = 4$–5 μm that exists for a wide range of f, and then stretches and flattens for higher f. Interestingly, the reason behind this bump is the dominance of the first transmission band under the emissivity curve for $d = 4$ μm (blue curve in Fig. 3). More specifically, below $d = 2$ μm, the first transmission band has not entered under the human body emissivity curve, yet gradually with increasing d it shifts to the right and overlaps. Around $d = 4$ μm, the majority of this band overlaps, leading to a higher τ bump. Furthermore, since the first transmission band shrinks with increasing f, the bump flattens for larger f. One has to keep in mind that, overall, increasing f decreases τ. The dip around $d = 6$ μm, immediately after the bump, is due to the structural band gap sliding under the emissivity curve. Upon further increasing f, the structural band gap shifts and is replaced by the second transmission band.

Figure 4(a) is a parameter framework that allows one to identify a specific range of parameters f and d that are suitable for a dynamic textile. Each τ point on the map corresponds to a certain d,f, and r, as $f = 2r/d$. Thus, for most variations in the map, the wire radius r changes, which is difficult in a practical realization. However, one can fix the radius r and assess the behavior of τ as a function of f and d. This is done by extracting τ from the map [Fig. 4(a)] for a fixed r, which gives a hyperbola when plotted as a function of f and d [see Fig. 1(a) within the Supplemental Material [42]].

In detail, in Fig. 4(b) we present τ as a function of d for various r. The arrow indicates the decreasing nature of τ with increasing r. Furthermore, the curve behaves differently for various d regions: for $d < 4$ μm, τ increases with a steep slope, then, around $d = 2$ to 6 μm, it flattens, and after $d > 6$ μm, starts to increase gradually. The steep slope indicates a very useful switching region with respect to the wire distance d. A change in d of approximately

2 μm for $r = 0.41$ μm results in a transmittance change of $\Delta\tau = 0.4$, and for $r = 0.07$ μm in a change of $\Delta\tau = 0.7$ for example.

In light of this, as a figure of merit, we introduce the derivative of τ with respect to d [see Fig. 1(b) within the Supplemental Material [42]]. The maximum of $d\tau/dd$ is plotted as a function of r in Fig. 4(c). For $r < 0.1$ μm, there is a very large value of $d\tau/dd$ (0.45–0.55 μm^{-1}), decreasing upon increasing r. This is because a smaller r corresponds to a smaller f, which results in a larger τ and $d\tau/dd$.

Now we can determine a suitable r for efficient operation: a very small r gives the largest and best $d\tau/dd$, and accordingly the best switching efficiency. The practical limit for the size of the monofilament diameter in current textile technology can go to the submicrometer scale. For example, for a carbon-based nanofiber, the reported diameter is around 200 nm [53]. If this is the fabrication limit, $r < 0.1$ μm is not practical. As a result, we use $r \geq 0.1$ μm, which corresponds to $d\tau/dd \leq 0.4$ μm^{-1} for the proposed fabric.

B. TM polarization

In this section, we analyze the electromagnetic response for TM polarization. Numerical spectra together with the human body emissivity are presented in Fig. 5. For longer wavelengths, unlike for TE polarization, there is no plasmonic gap. Instead, there is a transmission band followed by a structural band gap. Furthermore, this structural band gap has a strong dependence on f, and for larger f, this band gap becomes quite deep [see $f = 0.45$ (green curves) in Fig. 5]. Meanwhile, for smaller f, the structural band gap is weak and insignificant [see $f = 0.15$ (blue curves) in Fig. 5]. Furthermore, the spectra shift to the right (left) with increasing (decreasing) d.

In Fig. 6 we show the map of τ as a function of f and d. We can now divide this map into three regions: (i) where $f < 0.1$, (ii) where $f > 0.1$ and $d < 4$ μm, and (iii) where $f > 0.15$ and $d > 4$ μm. In regions (i) and (ii) τ is around 0.9 and, thus, close to a complete thermal transmission, which is in contrast with region (i) for TE polarization [see Fig. 4(a)], but analogous to region (iii) for TE polarization [very small f and very large d in Fig. 4(a)].

In region (i), with small f, the spectral transmittance is very high for longer wavelengths [see $f = 0.15$ (blue curves) in Fig. 5]. Furthermore, even though the spectral curve shifts to higher wavelengths with increasing d, as long as there is no strong structural band gap, which is the case for small f, τ stays the same and large (approximately 0.9).

Region (ii) also has a large τ: even though high f induces the geometric band gap, for small d, this gap is not yet under the human body emissivity curve [Fig. 5(a)]. Indeed, the spectral transmittance curve will not be the
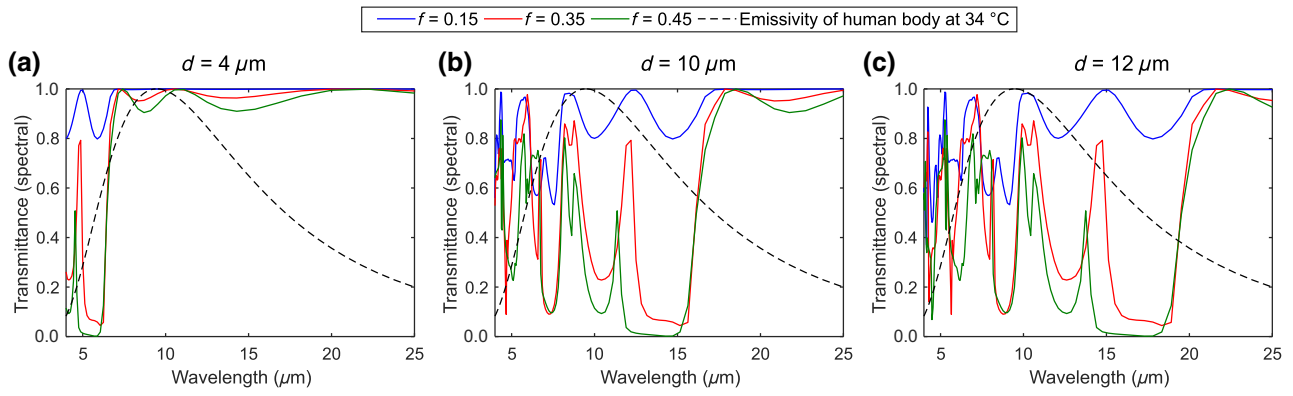
FIG. 5. TM transmittance spectra for $f = 0.15$, 0.35, and 0.45 μm, and (a) $d = 4$ μm, (b) $d = 10$ μm, (c) $d = 12$ μm. The dashed line depicts the human body emissivity at a skin temperature of 34 °C.

same for all f, but the overlap with the emissivity curve leads to very similar results.

In region (iii) τ starts to decrease gradually. There also exists a valley with its center around $d = 10$ μm for larger f, which flattens with decreasing f and increasing d. The valley appears because the structural band gap is strongly present for larger f. Shifting the spectral transmittance by changing d allows for a good overlap with the emissivity curve, which decreases τ. The center of the valley where τ is small is exactly when the structural band gap is completely under the emissivity curve. Increasing d further shifts the structural band gap to the right and finally out of the emissivity curve. Consequently, this allows the next transmission band to enter the curve, and thus τ increases, and the valley disappears.

C. Global design aspects

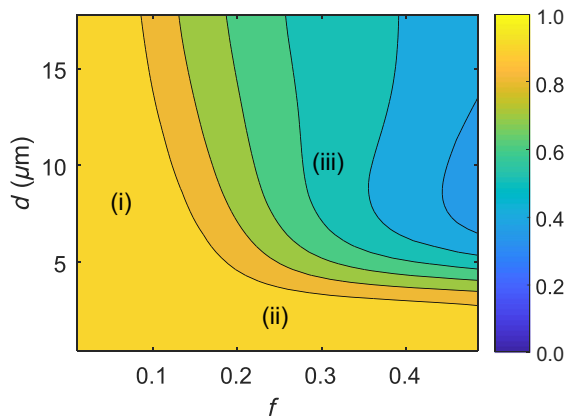Thermal radiation emitted by the human body is a largely incoherent, unpolarized electromagnetic wave,

consisting of both TE and TM components. So far, we have performed calculations for TE and TM polarizations independently, to identify the various photonic effects as a function of the geometric parameters. Here, we further assess these findings for flexible textiles. For example, we explore various monofilament configurations that could lead to a dynamic textile.

The TE calculations show a fortunate result, mainly due to the plasmonic gap and its dynamic response. Contrarily, since the plasmonic gap does not exist for TM polarization, it is not possible to utilize the same effect for both polarizations at the same time. However, to benefit both polarizations, a crossed array configuration provides a solution; see Fig. 7.

In the crossed case, the polarization component which is TE for the first array, becomes TM for the second array (and vice versa). Thus, if we use the edge of the plasmonic gap to modulate the transmission of the TE component via the first array, the transmission through the second array will be quasicomplete. Similarly, for the TM component,

FIG. 6. Spectrally integrated transmittance τ for TM polarization as a function of f and d.
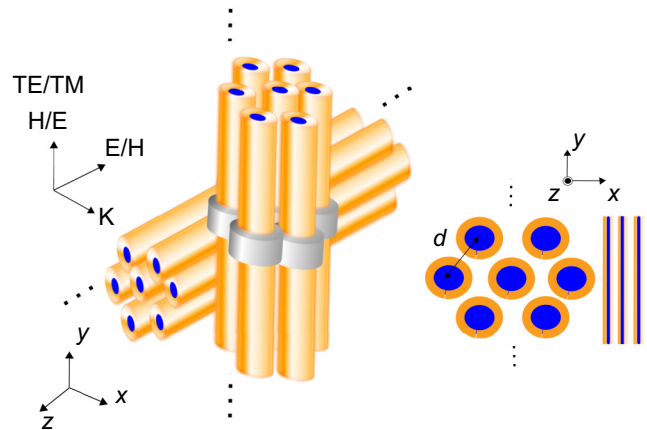

FIG. 7. Illustration of a crossed array configuration: (left) perspective and (right) planar view.

the transmission through the first array will be almost total, and the second array can be used to modulate the transmission (as TM becomes TE for the second array). In other words, a polarization modulated in the first array will be largely transmitted through the second array (and vice versa). We justify this reasoning using a three-dimensional (3D) simulation for the crossed array configuration (see Fig. 5 within the Supplemental Material [42]).

The crossed array can thus fully control the transmission of thermal radiation from the human body. It is also worthwhile to note that such a crossed nature is standard in textile production, especially for woven fabrics. As a result, in the next section, we discuss the thermal performance in two parts, for noncrossed (nonwoven) and crossed (woven) configurations.

The operational mechanism of the DTST design is tolerant to moderate amounts of disorder. Fundamentally, if some (or all) of the monofilaments are shifted from their original position, the crucial photonic effect that drives the operational mechanism (i.e., the plasmonic gap) is weakly affected (see Fig. 3 within the Supplemental Material [42]). It is expected that a substantial amount of disorder, such as removing some monofilaments or shifting them far from their original position, can disrupt the DTST function. However, careful integration of the design in a fabric should allow us to minimize the disorder to a tolerable extent. For example, one can configure the DTST fabric to be sandwiched between two separate layers of highly IR transparent fabric layers, made of woven fibers or aerogel material. This would further contribute to the mechanical rigidity, without distorting the radiative transfer channel.

In light of the TE and TM results, for the noncrossed (nonwoven) configuration, there is a possibility to exploit the structural band gap, as it exists in both polarizations. However, as can be seen from Figs. 4(a) and 6, the structural band gaps from the two polarizations do not align perfectly. As a consequence, the combined efficiency for thermal radiation suppression is relatively weak, so this configuration is not the best option for textile applications.

Examining a narrower wavelength range, however, allows for alternative dynamic IR filter applications. Furthermore, the dynamic contrast can be enhanced with more periods in the geometry. In Fig. 8(a) we show the spectrally integrated transmittance τ_n for a narrower wavelength range of the human body emissivity: from $\lambda_1 = 9.6$ μm to $\lambda_2 = 10$ μm [see Eq. (1)]. This time the design has an extra layer of wires [see the inset of Fig. 8(b)], leading to wider structural gaps, and the incoming radiation is considered unpolarized (we average TE and TM). The dark blue valley with low τ_n on the map around $d = 10$ μm is the result of the overlap of the structural band gaps for TE and TM polarizations. In Fig. 7(b) we show the gradient of τ_n for an optimized $r = 0.9$ μm, which shows a useful sharp change ($\Delta\tau_n = 0.6$) in the range of $d = 10$ to 12 μm. Thus, this design also functions as an efficient dynamic IR
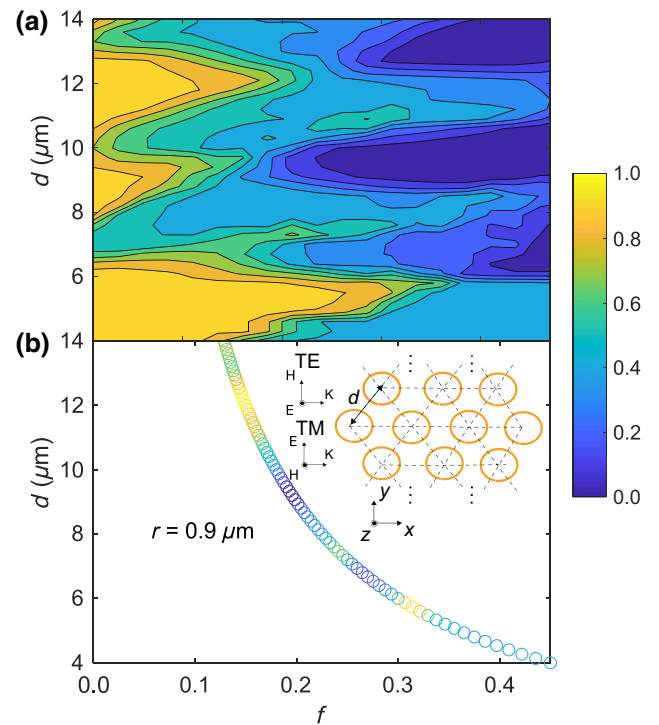

FIG. 8. (a) Spectrally integrated transmittance τ_n for a narrower wavelength range as a function of f and d. (b) Plot of τ_n for a constant radius $r = 0.9$ μm (inset shows the geometry, with an extra period).

filter, in this case around the human body peak emission wavelength (9.6 μm).

D. Thermal evaluation

We evaluate the thermal efficiency of the fabric based on a thermal model developed for this specific case (see the Appendix for details). This model builds upon the work of Siegel [54], who handled the radiative heat transfer between two opaque surfaces with a partially transparent nonabsorbing layer in between. We further extend this formalism to include both radiative and nonradiative heat transfer (i.e., conduction and convection) processes. Furthermore, the thickness of the fabric and air gap (microclimate) are taken into consideration. The main goal of the modeling is to determine the maximum and minimum surrounding environment temperatures that the textile can maintain without affecting the wearer's thermal comfort (i.e., the ambient setpoint temperature). Indeed, the user of a dynamic fabric can adapt to a wider ambient temperature range than with a static textile.

We assume a constant body heat generation of $Q = 70$ W/m^2, corresponding to a sedentary individual with a skin temperature of $34\,^\circ$C [23]. Thus, the equality between body heat generation and the sum of radiative, conductive, and convective heat flows defines the user's thermal comfort. We assume a typical air gap of 1 mm for the

microclimate thickness. Furthermore, the thermal conductivity of air is $k_{air} = 0.03$ Wm^{-2} K^{-1}, the effective thermal conductivity of fabric is $k_{DTST} = 0.05$ Wm^{-2} K^{-1} [55–57], the natural convection heat transfer coefficient is $h = 3$ Wm^{-1} K^{-1} [58], fabric thickness follows the relation $t_{DTST} = 2(d + r)$ (nonwoven) and $t_{DTST} = 4(d + r)$ (woven), the emissivity of the skin is approximated as a gray body with $\varepsilon_{skin} = 0.98$, the emissivity of the ambient environment is approximated as a black body with $\varepsilon_{amb} = 1$, and τ is retrieved from electromagnetic calculations for $r = 0.1$ μm, which we identified before as a suitable optimal size based on electromagnetic calculations and fabrication limits.

A typical setpoint temperature band for human thermal comfort in buildings, especially in offices, is subjective and requires polls and statistics in order to have a reliable value [59]; thus, here we consider a general average value of 22–24 °C for traditional textiles from the literature [60]. A lower setpoint corresponds to a better fabric heating performance, and a higher setpoint corresponds to a better cooling performance.

By using a DTST fabric, based on a crossed (woven) monofilament configuration, an expanded thermal comfort range with the lowest setpoint of 9.5 °C, and the highest setpoint of 25.7 °C, is achievable (Fig. 9). The lowest setpoint corresponds to τ close to zero, where $d = 1.2$ μm (expected maximum shrinking limit of polymer beads), and the plasmonic gap covers most of the human body emissivity curve; thus, the fabric is opaque to thermal radiation emitted by the human body. On the other hand, the highest setpoint achieved by the DTST corresponds to $\tau = 0.9$, where $d = 14$ μm (expected maximum swelling limit of polymer beads), and the second transmission band is the dominant photonic effect under the human body emissivity

curve; thus, the fabric is highly transparent to thermal radiation emitted by the human body. In addition, it is already possible to achieve a satisfactory highest setpoint temperature of approximately 24.5 °C with a limited swelling to only $d = 4$ μm, which corresponds to $\tau = 0.68$.

In comparison, the lowest setpoint is 4.8 °C lower than for the Mylar space blanket (14.3 °C) [61], 4.4 °C lower than for the dual-mode textile (13.9 °C) [31], and 5.2 °C lower than for the nanoporous metallized polyethylene textile (14.7 °C) in its cotton-polyethylene-Ag configuration [13]. Furthermore, the highest setpoint is 2.9 °C larger than that of cotton (22.8 °C), 1.4 °C more than for the dual-mode textile (24.3 °C) [31], and 0.6 °C more than for nanoporous polyethylene textile (25.02 °C) [23].

Accordingly, the dynamic woven configuration provides a very wide ambient setpoint temperature window of approximately 16 °C (Fig. 9). To our knowledge, the maximum reported setpoint window in both theoretical and fabricated textiles is 10.4 °C for passive (dual mode [31]) and 8.2 °C for active (squid skin inspired composite textile [9]) fabrics. In essence, this makes our proposal a very promising design, capable of preserving the thermal comfort of the wearer in a highly dynamic temperature situation, with fluctuations in the range of 9.5 to 25.7 °C.

On the other hand, for the noncrossed monofilament configuration, the thermal calculations still show an extended ambient setpoint temperature window of 6.9 °C (Fig. 9). The lowest setpoint is 19 °C and highest setpoint is 25.9 °C. As a result, the warming functionality of the design performs better than the Omni-Heat technology [62], a commercially available garment developed by Columbia Sportswear Company with a lower setpoint temperature of 20.6 °C. In addition, the cooling functionality performs better than the cooling mode of the dual-mode textile (24.3 °C for the higher setpoint) [31].

The envisioned DTST fabric could be made by utilizing micro- and nanofabrication techniques combined with standard textile manufacturing methods [19,27,30]. These techniques can vary from the very advanced 3D printing and core-shell electrospinning to the basic extrusion and dying processes. For example, Wang *et al.* [63] implemented the following. Firstly, they extruded a polymer from a spinneret to acquire the dielectric-core monofilament, which was subsequently drawn through a bath containing a metal solution. Secondly, they applied microwave radiation to facilitate the bonding of metal with the dielectric-core monofilament. Thirdly, the metal-coated monofilament passed through a bath with a stimuli-responsive polymer actuator solution to produce a layer containing the desired polymer beads. They controlled the polymer beads' size by adjusting the concentration, viscosity, and solvent component of the solution, or even by controlling the drawing velocity. In the end, various combinations of fabrication methods can be used
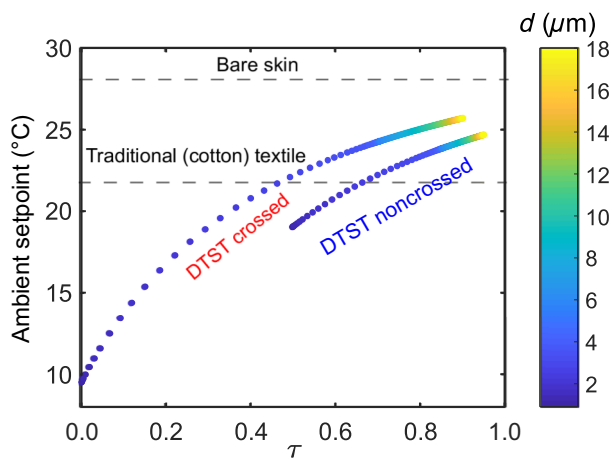

FIG. 9. Ambient setpoint temperature as a function of τ and d in crossed (dots above red font) and noncrossed (dots above blue font) configurations for $r = 0.1$ μm. The setpoint temperature values of bare skin and traditional (cotton) textile are also indicated.

to influence the design parameters, material choice, and efficiency.

IV. CONCLUSION

We demonstrate a personal radiative thermal regulating fabric based on a dynamic transmittance switch textile, using extensive electromagnetic and thermal calculations. The passive design with highly conducting wires benefits from various IR photonic effects to strongly control the wide-band transmission or reflection of thermal radiation. In the end, a very wide temperate setpoint window can be achieved, with the woven fabric configuration leading to approximately a $16\,^{\circ}$C setpoint window. The wearer is comfortable between 9.5 and $25.7\,^{\circ}$C, wider than any reported switchable fabric, active or passive. The proposed design is constituted from metal-coated monofilaments and stimuli-responsive polymer beads, which enables a passive dynamic response. Finally, the polyvalent structure can also be applied for narrowband, IR filter devices.

ACKNOWLEDGMENT

APPENDIX: THERMAL MODEL ANALYSIS

We consider thermal dissipation from the human body to the ambient environment as a one-dimensional steady-state heat transfer problem. Heat generated by the human body is lost by three different heat transfer processes (conduction, radiation, and convection); thus, the equality between total heat dissipation with total heat generation

$$Q_{\text{gen}} = Q_{\text{rad}} + Q_{\text{cond}} + Q_{\text{conv}} \qquad (A1)$$

leads to the user's thermal comfort [see Fig. 10(a)]. By implementing the well-established net radiation technique, Siegel [54] showed that the transfer between two opaque surfaces with a nonemitting layer in between is

$$Q_{\text{rad}} = \frac{\sigma (T_{\text{skin}}^4 - T_{\text{amb}}^4)}{1/\epsilon_{\text{skin}} + 1/\epsilon_{\text{amb}} + 1/\tau - 2}, \qquad (A2)$$

where $\sigma = 5.6 \times 10^{-8}$ W/m^{-2} K^{-4} is the Stefan-Boltzmann constant, T_{skin} is the skin temperature, T_{amb} is the ambient setpoint temperature, ϵ_{skin} and ϵ_{amb} are the emissivities of the skin and ambient environment, respectively. Conductive heat transfer through the air gap (microclimate) follows from Fourier's law:

$$Q_{\text{cond}}^{\text{air}} = \frac{k_{\text{air}}}{t_{\text{air}}}(T_{\text{skin}} - T_{\text{DTST}}^{\text{in}}); \qquad (A3)$$

conductive heat transfer through the fabric reads

$$Q_{\text{cond}}^{\text{DTST}} = \frac{k_{\text{DTST}}}{t_{\text{DTST}}}(T_{\text{DTST}}^{\text{in}} - T_{\text{DTST}}^{\text{out}}). \qquad (A4)$$

Here k_{air} and k_{DTST} are the thermal conductivity of air and effective thermal conductivity of the DTST fabric, t_{air} and t_{DTST} are the thicknesses of the air gap and DTST fabric, and $T_{\text{DTST}}^{\text{in}}$ and $T_{\text{DTST}}^{\text{out}}$ are the fabric's inner and outer side temperatures. The effective thermal conductivity of the DTST fabric is anisotropic and it consists of two components, k_z and k_x, in the directions parallel and perpendicular to the filaments' axis, respectively. The thermal conductivity in the longitudinal direction, i.e. the z direction with reference to Fig. 10(b), is given by

$$k_z = fk_m + (1 - f)\,k_{\text{air}}, \qquad (A5)$$

where f is the monofilament filling fraction, k_m and k_{air} are the thermal conductivities of the filament and air, respectively.

On the other hand, the thermal conductivity in the transverse direction, i.e., the x direction [Fig. 10(b)], can be
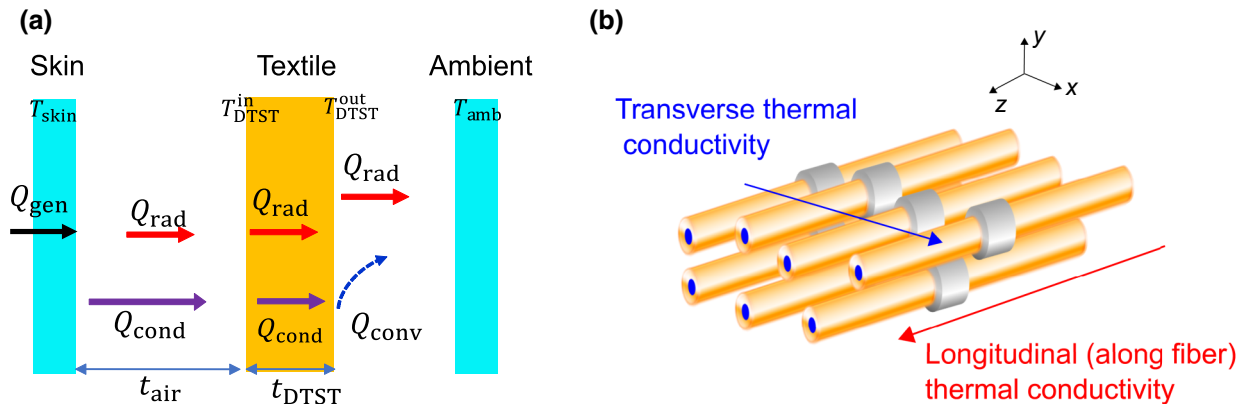

FIG. 10.   (a) Schematic of the heat transfer analysis. (b) Transverse and longitudinal thermal conductivity.

calculated using

$$\frac{1}{k_x} = \frac{f}{k_m} + \frac{1-f}{k_{air}}. \qquad (A6)$$

Since we are interested in 1D heat transfer from the human body to the ambient environment, only the transverse conductivity is considered in our heat transfer analysis (i.e., $k_{DTST} = k_x$). Note that, due to the dynamic nature of the DTST operation, the porosity of the design is not constant; however, we consider an average value in the thermal calculation [55–57,64,65]. Because of the small Rayleigh number in the air gap region, the convective heat transfer is negligible. However, convective heat transfer from the fabric outer surface to the ambient environment follows from Newton's law of cooling:

$$Q_{conv} = h(T_{DTST}^{out} - T_{amb}) \qquad (A7)$$

with h the convective heat transfer coefficient. A thermal balance combination of Eqs. (A2), (A3), (A4), and (A7) for the top surface, inside the fabric, and in the air gap allows one to calculate the ambient setpoint temperature.

The DTST is an IR transparent fabric, so the absorption or emission of the fabric is close to zero. Because of this, the amount of heat dissipation via radiation depends on the two emitters' temperature and emissivity (the human body and the ambient environment). However, with fixed skin temperature, fixed skin and ambient emissivities, the temperature of the ambient environment and transmittance of the fabric are the only factors that determine the radiative transfer. Thus, Q_{rad} in the air gap, inside the fabric, and in front of the fabric is the same. For example, if one considers the maximum cooling capability of the DTST (i.e., $T_{amb} = 25.9\,^\circ C$), Q_{rad} contributes approximately 90% of the total heat dissipation and $Q_{conv} = Q_{cond}^{air} + Q_{DTST}^{air}$ contributes the remaining approximate 10%. Indeed, this is expected since the DTST is highly transmitting in the cooling mode, and Q_{conv} and Q_{cond} depend linearly on the temperature gradient. On the other hand, in the heating mode, DTST transmittance is very low, and Q_{rad} contributes only approximately 10% of the total heat loss. While, with a higher temperature gradient, $Q_{conv} = Q_{cond}^{air} + Q_{cond}^{DTST}$ contributes the remaining approximate 90%. However, the above two examples are extreme cases; the dynamic nature of the DTST operation makes it hard to have static information about the various contributing heat transfer processes (i.e., with a different ambient temperature, the transmittance of the fabric changes, and, with it, the outer and inner side fabric temperatures).

The air gap (microclimate) thickness has a significant effect on controlling the conductive heat transfer. Indeed, a considerable thermal conductivity decrease can be achieved by increasing the gap between the skin and the textile. For example, one can increase the air gap thickness,

as long as the convective heat transfer in this region is negligible. Another solution is to add IR transparent material layers on the inner side of the fabric, which would cut conduction, while avoiding an increase in convection in the air gap.

[1] S. Banholzer, J. Kossin, and S. Donner, in *Reducing Disaster: Early Warning Systems for Climate Change* (Springer, 2014), p. 21.

[2] M. K. Van Aalst, The impacts of climate change on the risk of natural disasters, Disasters **30**, 5 (2006).

[3] B. Jones, B. C. O'Neill, L. McDaniel, S. McGinnis, L. O. Mearns, and C. Tebaldi, Future population exposure to us heat extremes, Nat. Clim. Chang. **5**, 652 (2015).

[4] A. J. McMichael, R. E. Woodruff, and S. Hales, Climate change and human health: Present and future risks, Lancet **367**, 859 (2006).

[5] G.-R. Walther, E. Post, P. Convey, A. Menzel, C. Parmesan, T. J. Beebee, J.-M. Fromentin, O. Hoegh-Guldberg, and F. Bairlein, Ecological responses to recent climate change, Nature **416**, 389 (2002).

[6] H. E. Murdock, D. Gibb, T. André, F. Appavou, A. Brown, B. Epp, B. Kondev, A. McCrone, E. Musolino, L. Ranalder *et al.*, Renewables 2019 global status report (2019).

[7] M. Beerepoot and A. Marmion, Policies for Renewable Heat: An Integrated Approach, type Tech. Rep. (OECD Publishing, 2012).

[8] J. D. Hardy and E. F. DuBois, Regulation of heat loss from the human body, Proc. Natl. Acad. Sci. USA **23**, 624 (1937).

[9] E. M. Leung, M. C. Escobar, G. T. Stiubianu, S. R. Jim, A. L. Vyatskikh, Z. Feng, N. Garner, P. Patel, K. L. Naughton, M. Follador *et al.*, A dynamic thermoregulatory material inspired by squid skin, Nat. Commun. **10**, 1 (2019).

[10] P.-C. Hsu, X. Liu, C. Liu, X. Xie, H. R. Lee, A. J. Welch, T. Zhao, and Y. Cui, Personal thermal management by metallic nanowire-coated textile, Nano Lett. **15**, 365 (2015).

[11] S. Jafar-Zanjani, M. M. Salary, and H. Mosallaei, Metafabrics for thermoregulation and energy-harvesting applications, ACS Photonics **4**, 915 (2017).

[12] P. B. Catrysse, A. Y. Song, and S. Fan, Photonic structure textile design for localized thermal cooling based on a fiber blending scheme, ACS Photonics **3**, 2420 (2016).

[13] L. Cai, A. Y. Song, P. Wu, P.-C. Hsu, Y. Peng, J. Chen, C. Liu, P. B. Catrysse, Y. Liu, A. Yang *et al.*, Warming up human body by nanoporous metallized polyethylene textile, Nat. Commun. **8**, 1 (2017).

[14] Y. Peng, J. Chen, A. Y. Song, P. B. Catrysse, P.-C. Hsu, L. Cai, B. Liu, Y. Zhu, G. Zhou, D. S. Wu *et al.*, Nanoporous polyethylene microfibres for large-scale radiative cooling fabric, Nat. Sustainability **1**, 105 (2018).

[15] L. Cai, A. Y. Song, W. Li, P.-C. Hsu, D. Lin, P. B. Catrysse, Y. Liu, Y. Peng, J. Chen, H. Wang *et al.*, Spectrally selective nanocomposite textile for outdoor personal cooling, Adv. Mater. **30**, 1802152 (2018).

[16] Z. Li, Z. Xu, Y. Liu, R. Wang, and C. Gao, Multifunctional non-woven fabrics of interfused graphene fibres, Nat. Commun. **7**, 1 (2016).

[17] T. Gao, Z. Yang, C. Chen, Y. Li, K. Fu, J. Dai, E. M. Hitz, H. Xie, B. Liu, J. Song *et al.*, Three-dimensional printed thermal regulation textiles, ACS Nano **11,** 11513 (2017).

[18] J. K. Tong, X. Huang, S. V. Boriskina, J. Loomis, Y. Xu, and G. Chen, Infrared-transparent visible-opaque fabrics for wearable personal thermal management, ACS Photonics **2,** 769 (2015).

[19] Z. Yu, Y. Gao, X. Di, and H. Luo, Cotton modified with silver-nanowires/polydopamine for a wearable thermal management device, RSC Adv. **6,** 67771 (2016).

[20] R. Liu, X. Wang, J. Yu, Y. Wang, J. Zhu, and Z. Hu, A novel approach to design nanoporous polyethylene/polyester composite fabric via tips for human body cooling, Macromol. Mater. Eng. **303,** 1700456 (2018).

[21] Y. Guo, C. Dun, J. Xu, J. Mu, P. Li, L. Gu, C. Hou, C. A. Hewitt, Q. Zhang, Y. Li *et al.*, Ultrathin, washable, and large-area graphene papers for personal thermal management, Small **13,** 1702645 (2017).

[22] K. Fu, Z. Yang, Y. Pei, Y. Wang, B. Xu, Y. Wang, B. Yang, and L. Hu, Designing textile architectures for high energy-efficiency human body sweat-and cooling-management, Adv. Fiber Mater. **1,** 61 (2019).

[23] P.-C. Hsu, A. Y. Song, P. B. Catrysse, C. Liu, Y. Peng, J. Xie, S. Fan, and Y. Cui, Radiative human body cooling by nanoporous polyethylene textile, Science **353,** 1019 (2016).

[24] L. Cai, Y. Peng, J. Xu, C. Zhou, C. Zhou, P. Wu, D. Lin, S. Fan, and Y. Cui, Temperature regulation in colored infrared-transparent polyethylene textiles, Joule **3,** 1478 (2019).

[25] H. Luo, Q. Li, K. Du, Z. Xu, H. Zhu, D. Liu, L. Cai, P. Ghosh, and M. Qiu, An ultra-thin colored textile with simultaneous solar and passive heating abilities, Nano Energy **65,** 103998 (2019).

[26] Q. Liu, J. Huang, J. Zhang, Y. Hong, Y. Wan, Q. Wang, M. Gong, Z. Wu, and C. F. Guo, Thermal, waterproof, breathable, and antibacterial cloth with a nanoporous structure, ACS Appl. Mater. Interfaces **10,** 2026 (2018).

[27] A. Hazarika, B. K. Deka, D. Kim, H. E. Jeong, Y.-B. Park, and H. W. Park, Woven kevlar fiber/polydimethylsiloxane/reduced graphene oxide composite-based personal thermal management with freestanding cu–ni core–shell nanowires, Nano Lett. **18,** 6731 (2018).

[28] K. Wu, L. Yu, C. Lei, J. Huang, D. Liu, Y. Liu, Y. Xie, F. Chen, and Q. Fu, Green production of regenerated cellulose/boron nitride nanosheet textiles for static and dynamic personal cooling, ACS Appl. Mater. Interfaces **11,** 40685 (2019).

[29] Y. Xu, B. Sun, Y. Ling, Q. Fei, Z. Chen, X. Li, P. Guo, N. Jeon, S. Goswami, Y. Liao *et al.*, Multiscale porous elastomer substrates for multifunctional on-skin electronics with passive-cooling capabilities, Proc. Natl. Acad. Sci. **117,** 205 (2020).

[30] X. A. Zhang, S. Yu, B. Xu, M. Li, Z. Peng, Y. Wang, S. Deng, X. Wu, Z. Wu, M. Ouyang *et al.*, Dynamic gating of infrared radiation in a textile, Science **363,** 619 (2019).

[31] P.-C. Hsu, C. Liu, A. Y. Song, Z. Zhang, Y. Peng, J. Xie, K. Liu, C.-L. Wu, P. B. Catrysse, L. Cai *et al.*, A dual-mode textile for human body radiative heating and cooling, Sci. Adv. **3,** e1700895 (2017).

[32] L. Ionov, Polymeric actuators, Langmuir **31,** 5015 (2015).

[33] A. Lendlein and O. E. Gould, Reprogrammable recovery and actuation behaviour of shape-memory polymers, Nat. Rev. Mater. **4,** 116 (2019).

[34] S. Chen, J. Hu, and H. Zhuo, Properties and mechanism of two-way shape memory polyurethane composites, Compos. Sci. Technol. **70,** 1437 (2010).

[35] M. Behl, K. Kratz, J. Zotzmann, U. Nöchel, and A. Lendlein, Reversible bidirectional shape-memory polymers, Adv. Mater. **25,** 4466 (2013).

[36] M. Behl, K. Kratz, U. Noechel, T. Sauter, and A. Lendlein, Temperature-memory polymer actuators, Proc. Natl. Acad. Sci. **110,** 12555 (2013).

[37] S. Shi, Q.-Y. Wu, L. Gu, K. Zhang, and H. Yu, Bio-based (co) polylactide-urethane networks with shape memory behavior at body temperature, RSC Adv. **6,** 79268 (2016).

[38] M. Sáenz-Pérez, T. Bashir, J. M. Laza, J. García-Barrasa, J. L. Vilas, M. Skrifvars, and L. M. León, Novel shape-memory polyurethane fibers for textile applications, Text. Res. J. **89,** 1027 (2019).

[39] L. Shuai, Z. Jun, C. Jianjun, Y. Ming, L. Xuepeng, and J. Zhiguo, Biodegradable body temperature-responsive shape memory polyurethanes with self-healing behavior, Polym. Eng. Sci. **59,** E310 (2019).

[40] M. Saatchi, M. Behl, U. Nöchel, and A. Lendlein, Copolymer networks from oligo (ε-caprolactone) and n-butyl acrylate enable a reversible bidirectional shape-memory effect at human body temperature, Macromol. Rapid. Commun. **36,** 880 (2015).

[41] G. Yang, X. Liu, A. I. Y. Tok, and V. Lipik, Body temperature-responsive two-way and moisture-responsive one-way shape memory behaviors of poly (ethylene glycol)-based networks, Polym. Chem. **8,** 3833 (2017).

[42] See the Supplemental Material at http://link.aps.org/supplemental/10.1103/PhysRevApplied.14.044030 for a spectral transmittance comparison between a real metal coating and perfect electric conductor, spectral transmittance for a disordered array, photonic band structure, and a spectral transmittance comparison between crossed wire (3D simulation) and noncrossed wire (2D simulation) configurations.

[43] O. Takayama and M. Cada, Two-dimensional metallo-dielectric photonic crystals embedded in anodic porous alumina for optical wavelengths, Appl. Phys. Lett. **85,** 1311 (2004).

[44] V. Kuzmiak, A. Maradudin, and F. Pincemin, Photonic band structures of two-dimensional systems containing metallic components, Phys. Rev. B **50,** 16835 (1994).

[45] M. M. Sigalas, C. T. Chan, K. Ho, and C. M. Soukoulis, Metallic photonic band-gap materials, Phys. Rev. B **52,** 11744 (1995).

[46] V. Kuzmiak and A. Maradudin, Photonic band structures of one-and two-dimensional periodic systems with metallic components in the presence of dissipation, Phys. Rev. B **55,** 7427 (1997).

[47] M. Shaban, A. M. Ahmed, E. Abdel-Rahman, and H. Hamdy, Tunability and sensing properties of plasmonic/1d photonic crystal, Sci. Rep. **7,** 1 (2017).

[48] A. H. Aly, M. Ismaeel, and E. Abdel-Rahman, Comparative study of the one dimensional dielectric and metallic photonic crystals, Opt. Photonics J. **2,** 105 (2012).

[49] J. D. Joannopoulos, S. G. Johnson, J. N. Winn, and R. D. Meade, *Molding the Flow of Light* (Princeton University Press, Princeton, NJ, 2008).

[50] L. Zhang, W. Yu, J.-Y. Ou, Q. Wang, X. Cai, B. Wang, X. Li, R. Zhao, and Y. Liu, Midinfrared one-dimensional photonic crystal constructed from two-dimensional electride material, Phys. Rev. B **98**, 075434 (2018).

[51] H. van der Lem and A. Moroz, Towards two-dimensional complete photonic bandgap structures below infrared wavelengths, J. Opt. A: Pure Appl. Opt. **2**, 395 (2000).

[52] D. L. Chan, M. Soljačić, and J. Joannopoulos, Thermal emission and design in one-dimensional periodic metallic photonic crystal slabs, Phys. Rev. E **74**, 016609 (2006).

[53] A. K. Yetisen, H. Qu, A. Manbachi, H. Butt, M. R. Dokmeci, J. P. Hinestroza, M. Skorobogatiy, A. Khademhosseini, and S. H. Yun, Nanotechnology in textiles, ACS Nano **10**, 3042 (2016).

[54] R. Siegel, *Net Radiation Method for Enclosure Systems Involving Partially Transparent Walls*, Tech. Rep. NASA TN D-7384 (NASA, Washington, DC, 1973).

[55] D. Jakšić and N. Jakšić, *Woven Fabric Engineering* (InTech, Rijeka, 2014), p. 255.

[56] R. Progelhof, J. Throne, and R. Ruetsch, Methods for predicting the thermal conductivity of composite systems: A review, Polym. Eng. Sci. **16**, 615 (1976).

[57] M. Wang, J. Wang, N. Pan, and S. Chen, Mesoscopic predictions of the effective thermal conductivity for microscale random porous media, Phys. Rev. E **75**, 036702 (2007).

[58] T. Mayor, S. Couto, A. Psikuta, and R. Rossi, Advanced modelling of the transport phenomena across horizontal clothing microclimates with natural convection, Int. J. Biometeorol. **59**, 1875 (2015).

[59] B. W. Olesen, Thermal comfort, Tech. Rev. **2**, 3 (1982).

[60] B. W. Olesen and K. Parsons, Introduction to thermal comfort standards and to the proposed new version of en iso 7730, Energy Build. **34**, 537 (2002).

[61] J. D. McCann, *Build the Perfect Survival Kit* (Penguin, New York, 2013).

[62] S. G. Hayes and P. Venkatraman, *Materials and Technology for Sportswear and Performance Apparel* (CRC Press, Boca Raton, 2016).

[63] Y. Wang, Composite Materials with Self Regulated Infrared Emissivity and Environment Responsive Fibers, Tech. Rep. Pub. No.: US 2016/0376747 A1 (United States Patent and Trademark Office, 2016).

[64] Z. Hashin, Analysis of properties of fiber composites with anisotropic constituents, J. Appl. Mech. Trans. ASME **46**, 543 (1979).

[65] J. Wang, J. K. Carson, M. F. North, and D. J. Cleland, A new approach to modelling the effective thermal conductivity of heterogeneous materials, Int. J. Heat. Mass. Transf. **49**, 3075 (2006).